Analyst

Accepted Manuscript

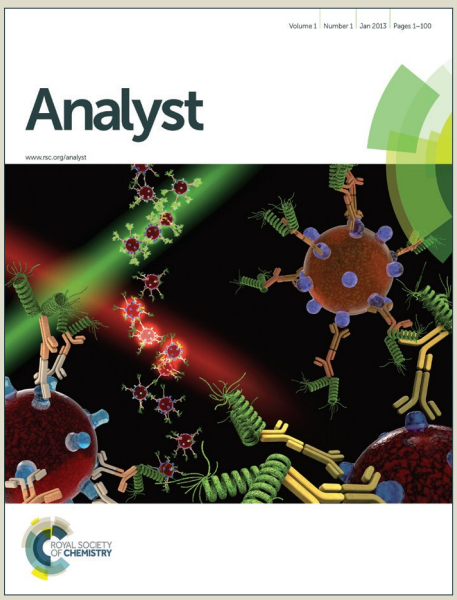

This is an *Accepted Manuscript*, which has been through the Royal Society of Chemistry peer review process and has been accepted for publication.

Accepted Manuscripts are published online shortly after acceptance, before technical editing, formatting and proof reading. Using this free service, authors can make their results available to the community, in citable form, before we publish the edited article. We will replace this *Accepted Manuscript* with the edited and formatted *Advance Article* as soon as it is available.

You can find more information about *Accepted Manuscripts* in the Information for Authors.

Please note that technical editing may introduce minor changes to the text and/or graphics, which may alter content. The journal's standard Terms & Conditions and the Ethical guidelines still apply. In no event shall the Royal Society of Chemistry be held responsible for any errors or omissions in this *Accepted Manuscript* or any consequences arising from the use of any information it contains.

ROYAL SOCIETY OF CHEMISTRY

www.rsc.org/analyst

Surfactant modulated aggregation induced enhancement of emission (AIEE) — a simple demonstration to maximize sensor activity

Rahul Bhowmick[a], Abu Saleh Musha Islam[a], Atul Katarkar[b], Keya Chaudhuri[b] and Mahammad Ali[a],*

[a]Department of Chemistry, Jadavpur University, 188, Raja Subodh Chandra Mallick Rd, Kolkata, West Bengal 700032, India, m_ali2062@yahoo.com

[b] Department of Molecular & Human Genetics Division , CSIR-Indian Institute of Chemical Biology , 4 Raja S.C. Mallick Road, Kolkata-700032, India

KEYWORDS: Rhodamine-based fluorophore; Turn-on dual sensor; SDS-templated microstructures; Cell imaging studies; Aggregation induced enhancement of emission (AIEE), SEM andTEM studies.

Abstract

A new type of easily synthesizable rhodamine-based chemosensor, **L**^{3}, with potential NO_2 donor atoms selectively and rapidly recognizes Hg^{2+} ion in presence of all biologically relevant metal ions and toxic heavy metals. Very low detection limit (78 nM) along with cytoplasmic cell imaging applications with no or negligible cytotoxicity provides a good opportunity towards *in-vitro*/ *in-vivo* cell imaging studies. SEM and TEM studies reveal a strongly agglomerated aggregation in presence of 5 mM SDS which turns into isolated core shell microstructures in

Analyst Accepted Manuscript

presence of 9 mM SDS. The presence of SDS causes enhanced quantum yield (φ) and stability constant (K_f) compared to those in absence of SDS. Again, the FI of $[\mathbf{L^3}–Hg]^{2+}$ complex in aqueous SDS (9 mM) medium is unprecedentedly enhanced (~143 fold) to that in absence of SDS. All these observations clearly manifest the enhanced rigidity of $[\mathbf{L^3}–Hg]^{2+}$ species in the micro-heterogeneous environment significantly restricting its dynamic movements. This phenomenon may be ascribed as an aggregation induced emission enhancement (AIEE). The fluorescence anisotropy assumes a maximum at 5 mM SDS due to strong trapping (sandwiching) of the doubly positively charged $[\mathbf{L^3}\text{-}Hg]^{2+}$ complex between two co-facial laminar microstructure of SDS under pre-miceller conditions where there is a strong electrostatic interaction that causes a better inhibition to dynamic movement of the probe-mercury complex. On increasing the SDS concentration there is a phase transition in SDS microstructures and micellization starts to prevail at SDS ≥ 7.0 mM. The doubly positively charged $[\mathbf{L^3}\text{-}Hg]^{2+}$ complex is trapped inside the hydrophobic inner core of the micelle which is apparent from the failure to quench the fluorescence of the complex on adding 10 equivalents of H_2EDTA^{2-} solution but in absence of SDS it is quenched effectively.

Introduction

In nature, there is a continuous drive of a web of chemical reactions of elements, ions and molecules.[1] Living organism and their environment interact with each other through a diverse array of reactions spanning from covalent to non-covalent interactions like electrostatic, hydrophobic, van der Waals, hydrogen bonding etc.[2,3] and a significant progress in designing and fabrication of appealing supramolecular assemblies have been achieved by chemists through bottom-up approach by elegant utilization these non-covalent interactions, which lead to

Analyst Accepted Manuscript

successful fabrication of optical materials and advanced nano-devices. It involves coupling of structurally different building blocks (ionic pairs) by electrostatic interactions.[3] Various combinations between polyelectrolytes, peptides, surfactants and extended rigid organic scaffolds could be employed for creating new material via ionic self-assembly.[4-9] Another promising feature of these supramolecular assemblies in concern is their emissive behavior in solution and solid states. The assemblies thereby formed may exhibit either aggregation caused quenching (ACQ) or aggregation induced emission enhancement (AIE or AIEE);[10-17] the later shows enhanced fluorescence emission efficiency in an aggregated state as compared to that in a solution state. In this context, AIEE phenomena became a key point in developing materials for fluorescent sensors, optoelectronic devices, and cell imaging applications. Up to now, the AIEE mechanism has been observed in silole derivative,[18] 1,1,2,2-tetraphenylethene (TPE),[19-22] 1-cyano-trans- 1,2-bis-(4-methylphenyl) ethylene (CN-MBE),[23,24] which were claimed to be a stimuli responsive material capable of detecting volatile organic vapor, biological polymer, pH changes, explosives, metal ions etc.

Fluorescence efficiency greatly depends on a number of factors that maximize the stability of a fluorophore in the excited state and minimize various non-radiative decay processes such as intermolecular interaction,[25] intramolecular charge transfer,[26,27] intramolecular torsional and rotational motions.[28-30] One of the ways to do so is to confine a probe by changing the outside environments which significantly deactivate these non-radiative decay processes and enhance the fluorescence efficiency − a way to develop organic light-emitting diodes for practical applications.[31,32] Thus, a number of fluorescent molecules exhibit aggregation-induced emission (AIE) properties by restricting the intramolecular vibrational, rotational, and torsional motion resulting a turned on or enhanced fluorescence[33] Obvious choice is to use ionic

Analyst Accepted Manuscript

surfactants where electrostatic interactions with a charged fluorescent probe suppress the nonradiative decay and hence enhance the fluorescence emission efficiency. Surfactants generally form micelles, vesicles, and other kinds of aggregates,[34] and therefore could be a good choice to modulate the aggregation of ionic fluorescent dyes in water and to adjust the fluorescence intensity. All these have found applications in biochemistry, analytical chemistry, and photosensitization.[35-37] However, only few reports are available where the induced fluorescence enhancement of dye molecules by surfactants occurs.[38-42]

Again, pollution due to heavy metals like mercury arises due to its wide scale applications in agriculture and industry. It is also widespread in air, water and soil by the oceanic and volcanic eruptions, combustion of fossil fuels, gold mining and solid waste incineration and seems to be inescapable.[43-45] As an example of highly toxic and widespread pollutants is the water-soluble Hg^{2+} ion, which can damage the brain, nervous system, kidneys, and endocrine system. In living organism Hg^{2+} deactivates many enzymes due to its strong affinity for sulfur in -SH groups which stops or alter the metabolic processes[46,47] As a result accumulation of Hg^{2+} in the body various disease like prenatal brain damage, serious cognitive and motion disorders, Mina Mata etc are common.[48]

Though there are several sophisticated analytical instruments like atomic absorption and emission spectroscopy,[49] inductively coupled plasma mass spectroscopy (ICP-MS),[50] inductively coupled plasma atomic emission spectrometry (ICP-AES)[51],voltammetry[52] etc are used for Hg^{2+} detection; however, most of these methods are either very costly or time-consuming and not suitable for performing assays. However, quick response, high sensitivity and good selectivity make fluorescence technique superior to others and attract tremendous research attention of chemists, biologists and environmentalists.[53-59]

Analyst Accepted Manuscript

Special structural features along with good photo stability; a high molar extinction coefficient and a longer emission wavelength (550 nm) make rhodamine a good choice for the construction of OFF–ON fluorescent chemosensors[51] to avoid background fluorescence below 500 nm.[53,60,57] Here, a new rhodamine-based probe with potential NO_2 donor atoms has been synthesized and successfully employed for the selective and rapid recognition of toxic Hg^{2+} ions (**Scheme 1**) in 8:2 (H_2O:MeCN) medium. It exhibits very rapid chromo- and fluorogenic OFF-ON responses through metal-induced opening of the spirolactam ring. Not only that, in aqueous SDS medium it was found to exhibit aggregation induced emission enhancement (AIEE)**.**

Experimental Section

Materials and Instruments:

Rhodamine 6G hydrochloride, 2-Chloro-N,N-diethylamine hydrochloride and metal salts such as perchlorates of Na^+, K^+, Ca^{2+}, Fe^{2+}, Co^{2+}, Ni^{2+}, Zn^{2+}, Pb^{2+}, Cd^{2+}, Hg^{2+} and Cu^{2+} and anions such as SO_4^{2-}, NO_3^-, PO_4^{3-}, S^{2-}, Cl^-, F^-, Br^-, OAc^-, $H_2AsO_4^-$, N_3^-, ClO_4^-, PPi, $S_2O_4^{2-}$, HCO_3^-, SCN^-, CO_3^{2-}, $P_2O_7^{4-}$ and NO_2^- were purchased from Sigma–Aldrich and used as received. All solvents used for the synthetic purposes were of reagent grade (Merck) unless otherwise mentioned. For spectroscopic (UV/Vis and fluorescence) studies HPLC-grade MeCN and deionized water from MiliQ Millipore were used.

UV/Vis absorption spectra were recorded on an Agilent 8453 diode array spectrophotometer. Steady-state fluorescence studies were carried out with a PTI (QM-40) spectrofluorimeter. NMR spectra were recorded on a Bruker spectrometer at 300 MHz. The ESI-MS^+ spectra were recorded on a Waters XEVO G2QTof mass spectrometer.

Analyst Accepted Manuscript

Preparation of Rhodamine 6G Hydrazide (L^1)

Rhodamine-6G hydrazide was prepared according to a literature method.[61]

Preparation of 2-[2-(diethylamino)-ethoxy]-5-nitro-benzaldehyde (L^2).

In a typical procedure 5-nitro salicylaldehyde (5 mmol, 0.835 g) was dissolved in dry MeCN (30 mL) to which K_2CO_3 (6 mmol, 0.3312 g) was added, and the mixture was heated at reflux for 40 min. 2-Chloro-N,N-diethylamine hydrochloride (6 mmol, 1.032 g) was then added and reflux was continued for another 5 h. It was then cooled to room temperature and filtered. The filtrate was evaporated to one third of its initial volume and diluted with 40 mL water. The pH of the resulting solution was then adjusted to 4 by the addition of 1 M HCl and extracted with dichloromethane (DCM; 2 x 40 mL). The pH of the aqueous solution was further adjusted to 8 by the addition of 4.0 M Na_2CO_3 solution and again extracted with DCM (3 x 40 mL). The combined organic phase was dried over anhydrous Na_2SO_4 and then evaporated to dryness under reduced pressure to afford a reddish yellow solid. The solid product was recrystallized from MeCN/DCM (8:2, v/v) to give the **L^2** as amorphous solid.

Preparation of L^3.

2-[2-(diethylamino)-ethoxy]-5-nitro-benzaldehyde (**L^2**) (1.10 mmol, 0.266 g) in MeOH (10 mL) was added dropwise to a methanolic solution (30 mL) of **L^1** (1 mmol, 0.464 g) containing 1 drop of acetic acid under hot (50–60 °C) conditions over 30 min and it was then stirred for about 6 h at room temperature whereupon yellow precipitate formed was collected by filtration. The residue was washed thoroughly with cold methanol to isolate **L^3** in pure form in 78% yield. The detail synthetic steps are illustrated in **Scheme 1**.

Analyst Accepted Manuscript

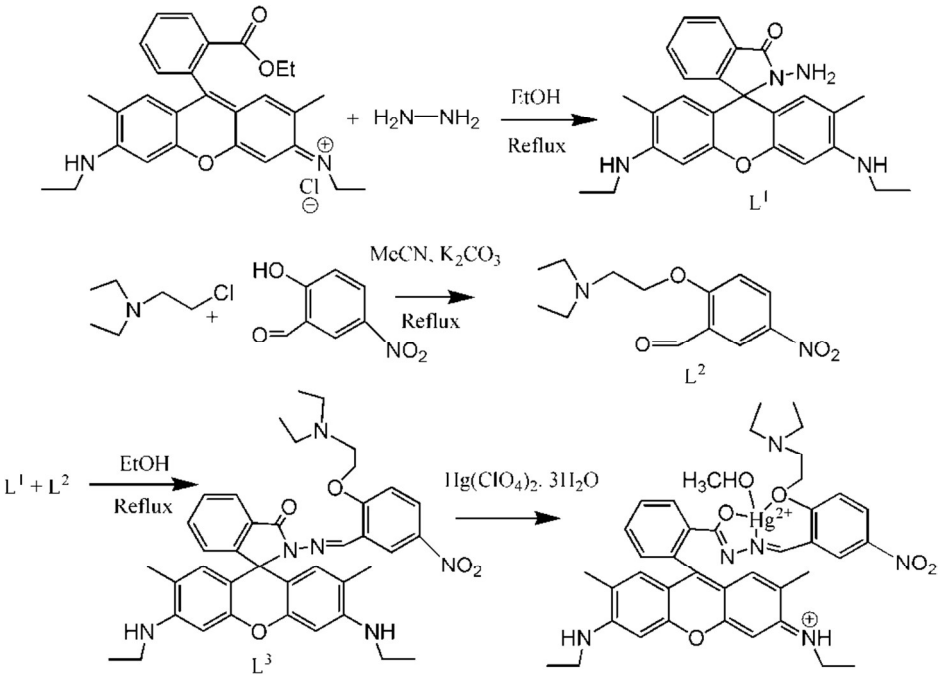

Scheme 1

Analysis.

^{1}H NMR (DMSO-d_6): δ = 8.83(s, 1 H), 8.31 (s, 1 H), 8.04 (s, 1 H), 7.92 (s, 1 H), 7.58 (m, 2 H), 7.03(d, 1-H), 6.92 (d, 1 H), 6.30 (s, 2 H), 6.16 (s, 2 H), 5.07 (t, 2 H), 3.11(t, 4 H), 2.48 (s, 14 H), 1.82 (s, 6H), 1.18 (t,6H) ppm **(Fig. S1)**. IR: $\tilde{\nu}$ = 1722 cm^{-1} (spirolactam amide-keto), 1622 cm^{-1} (–C=N) (**Fig. S2**). MS (ES$^+$): *m*/*z*=677.4009 [L+H$^+$] (**Fig. S3**).

Preparation of complex L^3-Hg^{2+}

$Hg(ClO_4)_2$ (0.272 g, 0.6 mmol) was added to a 10 mL MeCN solution of **L^3** (0.338g, 0.5 mmol) and the mixture was stirred for about 30 minutes. It was then filtered and allowed to evaporate slowly at ambient temperature to get crystalline solid product.

Analyst Accepted Manuscript

Analysis: ^{1}H NMR (DMSO-d_6): δ = 8.83(s, 1 H), 8.29 (d, 1H), 8.05 (d, 1 H), 8.03 (d, 1 H,), 7.60 (m, 2 H), 7.03 (d, 1 H), 6.92 (d, 1 H), 6.35 (s, 2 H), 6.18 (s, 2 H),5.45 (s, 1 H),3.12 (m, 4 H), 2.48 (s, 14 H), 1.83 (s, 6 H), 1.18 (t, 6 H) ppm (**Fig. S4**). IR: $\tilde{\nu}$ = 1633cm^{-1} (spirolactam ring open), 1608cm^{-1} (–C=N) (**Fig. S2**). MS (ES$^+$): *m*/*z* = 532.5052 (**L^3**+Hg^{2+}+ClO_4+H_2O+ CH_3OH+CH_3CN) and 629.4355 (**L^3**+Hg^{2+}+$(ClO_4)_3$+ $(H_2O)_3$+Li_2) (**Fig. S5**).

Solution Preparation for UV-Vis and fluorescence studies

For both UV-Vis and fluorescence studies, a stock solution 1.0 x 10^{-3} M of **L^3** was prepared by dissolving required amount of ligand in 2 ml MeCN and finally the volume was adjusted to 10 ml by de-ionized water. In a similar way, 1.0 x 10^{-3} M stock solution of Hg^{2+} was prepared in de-ionised H_2O. A 250 mL 10 mM HEPES buffer solution in 8:2 H_2O:MeCN (v/v) was prepared and pH was adjusted to 7.2 by using HCl and NaOH. 2.5 ml of this buffer solution was pipetted out into a cuvette to which required volume of 1.0 x 10^{-3} M probe was added to achieve 20 μM and 10 μM final concentrations for UV-Vis and fluorescence titration, respectively. In a regular interval of volume of Hg^{2+} ions were added incrementally and UV-Vis and fluorescence spectra were recorded for each solution. The cuvettes of 1 cm path length were used for absorption and emission studies. Fluorescence measurements were performed using 2 nm x 2 nm slit width.

Preparation of sample for SEM and TEM studies

We prepared 10 mL 1 mM stock solution of the ligand and 10 ml 0.10 M stock solution of SDS. Now, 25 μL of the ligand solution was added to (a) 125 μL and (b) 225 μL SDS solution in 2.5 mL deionized water with stirring for 5 minutes. The concentrations of SDS/L^3 in the resulting solutions were (a) 5.0/0.10 mM and (b) 9.0/0.10 mM respectively. The use of higher

Analyst Accepted Manuscript

concentration of SDS (upto 20 mM) does not show the formation of microstructure. We have prepared another set of solutions (a) and (b) with appropriate amount of ligand (25 μL) and to each solution 1 equivalent of Hg^{2+} was added. All the solutions were aged overnight at room temperature before characterization. The samples in both cases were found to give best microstructure as analyzed by SEM and TEM studies.

Methods of Characterization

The morphologies of the synthesized nano/micro structures were studied using a ZEOL, JSM 8360 scanning electron microscope (SEM) operated at an accelerating voltage of 5 kV. Before SEM studies, the samples were vacuum dried on a glass plate and deposited as a thin layer of carbon. Transmission Electron Microscope (TEM) studies were performed on a JEOL JEM 2100 HR with EELS operating between accelerating voltage of 80KV to 200 KV. The sample was deposited on a copper grid and vacuum dried.

Steady-state fluorescence and fluorescence anisotropy were measured with a PTI QM-40 spectrofluorometer. Fluorescence anisotropy (r) is defined as:

$$r = (I_{VV} - G \cdot I_{VH})/(I_{VV} + 2G \cdot I_{VH}) \quad (1)$$

where, I_{VV} and I_{VH} are the emission intensities obtained with the excitation polarizer oriented vertically and emission polarizer vertically and horizontally, respectively. The G factor is defined as[53]

$$G = I_{HV}/I_{HH} \quad (2)$$

where, the intensities I_{HV} and I_{HH} refer to the vertical and horizontal positions of the emission polarizer, with the excitation polarizer being horizontal.

Analyst Accepted Manuscript

Cell culture

Human hepatocellular liver carcinoma (HepG2) cell lines were procured from NCCS (Pune). The cells were cultured in DMEM (penicillin-100 μg/ml, 10% FBS, streptomycin-50 μg/ml) at 37ºC in 95% air, 5% CO_2 incubator.

Cell viability Assay

To determine % cell viability the colorimetric MTT assay of ligand $\mathbf{L^3}$ was performed by the method reported earlier.[62]

Cell Imaging Study

1×10^5 cells were cultured and incubated over coverslip in 35x10 mm culture dish for 24h at 37°C. The cells were treated with 10 μM $\mathbf{L^3}$ (prepared by dissolving $\mathbf{L^3}$ to the mixed solvent DMSO: water = 1:9 v/v) and then allowed to incubate for 45 min at 37 °C. After incubation cells were incubated with MitoTracker® Green FM (Invitrogen) for 30 min to track the cytoplasm followed by washing thrice with 1X PBS. This was allowed to counterstained by DAPI (2-(4-Amidinophenyl)-6-indolecarbamidine dihydrochloride, 4′,6-Diamidino-2-phenylindole, used for nuclear staining, Sigma). Fluorescence images of HepG2 cells were taken by a fluorescence microscope (Leica DM3000, Germany) with an objective lens of 40X magnification. Additionally, fluorescence images of HepG2 cells were taken, where cells were pre-incubated with 2 μM, 4 μM, 8 μM, 16 μM, 20 μM Hg^{2+} for 3h in three different culture dishes at 37^0C followed by washing thrice with 1X PBS and incubated with equimolar amount of ligand $\mathbf{L^3}$ (2 μM, 4 μM, 8 μM, 16 μM, 20 μM respectively) for 30 min at 37^0C. After incubation, cells were washed with 1X PBS three times and fluorescence images were taken. $\mathbf{L^3}$ shows intracellular

Analyst Accepted Manuscript

cytoplasmic red fluorescence by forming complex with Hg^{2+} against the nuclear counterstain DAPI (blue color) and cytoplasmic stain MitoTracker Green (Green color).

Results and Discussion

A Schiff base condensation between L^1 and L^2 in methanol (Scheme 1) under refluxing conditions affords L^3, which was thoroughly characterized by ^{1}H-NMR, IR and ESI-MS$^+$ spectroscopy.

Absorption and Steady-State Emission Studies

The UV-Vis titration with fixed concentration of L^3 (20 μM) with variable concentration of Hg^{2+} (0 – 25.0 μM) at 25 °C in aqueous MeCN (8:2, v/v, HEPES buffer, pH 7.2) showed a gradual development of a new absorption band at around 533 nm on addition of Hg^{2+} (Fig. 1).

Fig. 1

A plot of absorbance vs. [Hg^{2+}] **gives a non-linear curve (**Fig. 7) with decreasing slope and can be analyzed by using equation (1)[63] below. The binding constant of the formed complex L^3–Hg^{2+} was determined to be K_f = (2.39 ± 0.49) x 10^4 M^{-1}.

$$y = \frac{a + b\,x^n}{1 + c\,x^n} \qquad (1)$$

where, a = absorption minimum (A_{min}), b= absorption maximum (A_{max}) and c = K_f = apparent formation constant.

Analyst Accepted Manuscript

Job's method was employed to determine the composition of the complex which was found to be 1:1 (Fig. 1c). The emission spectra of L^3 and its fluorescence titration with Hg^{2+} were performed in water:MeCN (8:2, v/v) solution with fixed concentration of L^3 (10 μM) (10 mM HEPES buffer, pH 7.2; Fig. 2). On gradual addition of Hg^{2+} (0–56.0 μM) to the non-fluorescent solution of L^3 (10.0 μM), a 316-fold enhancement in fluorescence intensity at 553 nm was observed following excitation at 510 nm, which also suggests the opening of the spirolactam ring in L^3 on coordination to the Hg^{2+} ion.

Fig. 2

A plot of FI vs. $[Hg^{2+}]$ gives a straight line upto 50 μM where, the eqn.(1) becomes y = a+b*c*x under the conditions 1>>c*x and linear dependence of such plot gives slope = b*c, where, b= fluorescence maximum (F_{max}) and c = $K_{f'}$ = apparent formation constant. So, slope/F_{max} gives $K_{f'}$ = (2.02 ± 0.03) x 10^4 M^{-1}. It is interesting to note that the values of $K_{f'}$ **obtained separately from absorbance and fluorescence titrations are very close to each other and clearly indicate the self-consistency of our results.**

The detection of Hg^{2+} was not affected by the presence of biologically abundant metal ions like Na^+, K^+, Ca^{2+} and Mg^{2+}. Likewise, under identical reaction conditions no significant color or spectral change was observed for transition-metal ions, namely Cr^{3+}, Mn^{2+}, Fe^{2+}, Fe^{3+}, Co^{2+}, Cu^{2+}, Ni^{2+} and Zn^{2+}, and heavy-metal ions, like $Cd^{2+}$and Pb^{2+} and also anions like SO_4^{2-}, NO_3^-, PO_4^{3-}, S^{2-}, Cl^-, F^-, Br^-, OAc^-, H_2AsO^{4-}, N_3^-, ClO_4^-, PPi, $S_2O_4^{2-}$, HCO_3^-, SCN^-, CO_3^{2-}, $P_2O_7^{4-}$ and NO_2^- (**Fig. 3**).

Analyst Accepted Manuscript

We have also checked the thiophilicity of Hg^{2+} ions using cysteine under extracellular conditions. It was observed that the probe undergoes complete fluorescence quenching on addition of thiol (10 μM) to an ensemble of 10 μM $\mathbf{L^3}$-Hg^{2+}. This clearly indicates that the probe could be used to detect Hg^{2+} as well as thiols to the concentration of at least 10 μM which are best viewed in **Fig. S6**. The quantum yield (φ) of the free ligand and L3—$Hg2^{+}$ complex in pure water in absence and presence of 9 mM SDS are determined which were found to be: 0.0029 (L^3); 0.11 (L^3 in presence of 9 mM SDS); 0.009 (L^3 in presence of 1.2 equivalent of Hg^{2+}) and 0.48 (L^3 + 9 mM SDS + 1.2 equivalent Hg^{2+} in pure water. The life time of the free ligand in absence and presence of SDS (9 mM) are 0.41 and 3.33 ns respectively while that of $\mathbf{L^3}$-Hg^{2+} complex are 4.51 and 3.31 ns respectively.

Fig. 3.

pH Stability Check. The pH-titration over a wide range of pH (2-12) reveals no obvious fluorescence emission of $\mathbf{L^3}$ between pH 4 and 12. However in presence of Hg^{2+} it becomes fluorescent between the pH 6.5-12 suggesting a convenient application of this probe under physiological conditions (**Fig. 4**).

Fig. 4

Determination of LOD. The 3σ method was adopted to determine the limit of detection (LOD) of Hg^{2+} and was found to be as low as 78 nM (**Fig 5**) which indicates that $\mathbf{L^3}$ is an ideal chemosensor for Hg^{2+} ion.

Fig. 5

Analyst Accepted Manuscript

Mechanism of ring opening.The characteristic stretching frequency of the amidic "C=O" of the rhodamine moiety at 1722 cm^{-1} is shifted to a lower wave number (1633 cm^{-1}) in the presence of 1.2 equiv. of Hg^{2+} (**Figure S2**) indicating a strong polarization of the C=O bond upon efficient binding to the Hg^{2+} ion; and in fact, indicates the cleavage of N-C bond in spirolactum ring. Also, the ^{1}H NMR spectra showed an up-field shift for azomethine proton mainly due to an increase in electron density arising from the opening of the spirolactam ring.

Steady-State Fluorescence studies in presence of SDS.

Steady state fluorescence studies were also carried out in presence of SDS under two experimental conditions. Firstly, SDS concentration was kept fixed at 9 mM and [Hg^{2+}] was varied between 0 and 14 μM keeping [L^3] = 10 μM (**Fig. 6a**). A plot of FI vs. [Hg^{2+}] resulted a non-linear curve (**Fig. 6b**) and was solved by adopting eqn 1. The evaluated K_f value (4.19 ± 0.02) x 10^5 M^{-1} was found to be about one order of magnitude higher than that obtained in the absence of SDS. In order to get the SDS dependent K_f values we have varied [Hg^{2+}] at different concentration of SDS and thereby evaluated K_f values were plotted against the concentration of [SDS]. It was interesting to observe that there is a slow but gradual increase in K_f values with [SDS] upto 6 mM and a further increase in [SDS] there is a steep rise in K_f value up to 9 mM (**Fig. 7**).

Fig. 6

Fig.7

Analyst Accepted Manuscript

This enhanced stability constant value may be attributed to the restriction to the free dynamic movement of the doubly positively charge [$\mathbf{L}^3$–Hg]$^{2+}$ complex by the strong electrostatic attraction with the negatively charged head groups of SDS.

Secondly, both [$\mathbf{L}^3$] and [Hg^{2+}] were kept fixed at 10 μM and [SDS] was varied between 0 and 10 mM which yielded a non-linear curve on plotting FI vs. [SDS] gives a plateau at [SDS] ~ >9.0 mM with a fluorescence enhancement of ~143 fold with respect to the complex in absence of SDS (**Fig. 8**). The appearance of a plateau at ~9 mM SDS clearly indicates a critical micellar concentration (CMC) of SDS is ~9.0 mM under the experimental conditions. The increase in FI with [SDS] manifests the fact of aggregation induced enhancement (AIE) of

Fig. 8

fluorescence. The binding of $\mathbf{L}^3$–Hg^{2+} to anionic sulfonic acid groups via electrostatic interactions was confirmed by the failure to observe any change in fluorescence intensity in presence of cetyltrimethylammonium bromide (CTAB) – a cationic surfactant.

On the basis of these observations, it is concluded that the intermolecular electrostatic interaction between [$\mathbf{L}^3$–Hg^{2+}] and SDS may effectively lower the dynamic motion and decrease the non-radiative decay process and hence increase in fluorescence intensity, quantum yield (φ) and stability constant (K_f) values compared to the respective values in the absence of SDS.

Steady-State Fluorescence Anisotropy Measurements.

Steady-state fluorescence anisotropy can be exploited to get motional information in the micro heterogeneous environments.[62] We have monitored the fluorescence anisotropy(r) as a function of SDS concentration (0-10 mM) at a fixed concentration of $\mathbf{L}^3$ and Hg^{2+} (10 μM each) at 553

Analyst Accepted Manuscript

nm. A plot of r vs. [SDS] showed a gradual increase in r with [SDS], reaches a maximum at ~5 mM and then decreases upto 5.5 and again increases with [SDS] and becomes constant at [SDS] ≥7.0mM. This unusual dependence of r on SDS concentration can be rationalized by considering the fact that initial increase in r is due to trapping of the bi-positive [$\mathbf{L^3}$-Hg]$^{2+}$ complex between to co-facial laminar layers which mostly prevailed within 3.0-5.5 mM concentration of SDS (Scheme 2). The decrease in r after 5.0 mM may arise due to phase transition and again further increase in r may be due to the formation of spherical aggregates upon micellization at ~ 7.0 mM of SDS and after that the r values become almost constant. The variation of fluorescence anisotropy (r) as a function of SDS concentration is presented in **Fig. 9.**

To verify whether the probe is trapped inside the hydrophobic core of the micelle or it remains in the Stern-Volmer layer we have carried out fluorescence quenching experiment by EDTA in presence of SDSof5 mM and 9 mM concentrations and also in the absence of SDS. It was interesting to note that there is no practical quenching of fluorescence intensity of $\mathbf{L^3}$-Hg^{2+} complex on adding 10 equivalents of H_2EDTA^{2-} in presence of 9 mM SDS; howeverit undergoes a fluorescence quenching by ~ 50% of its original value in presence of 5 mM SDS and 100% quenching occurs when practically there is no SDS in the solution (**Fig. S7**). All these observations indicate the non-accessibility of $\mathbf{L^3}$-Hg^{2+} complexes towards H_2EDTA^{2-} surely due to trapping of $\mathbf{L^3}$-Hg^{2+} in the hydrophobic core of the spherical micelle when SDS concentration is 9 mM. But partial availability of $\mathbf{L^3}$-Hg^{2+} towards H_2EDTA^{2-} occurs when it is sandwiched in the hydrophilic region between two co-facial laminar layers. We have also carried out SEM and TEM studies on the aggregates at 5.0 mM and 9.0 mM of SDS to support the above proposition and indeed there is some positive indication (Figure 10 and 11).

Fig. 9

Analyst Accepted Manuscript

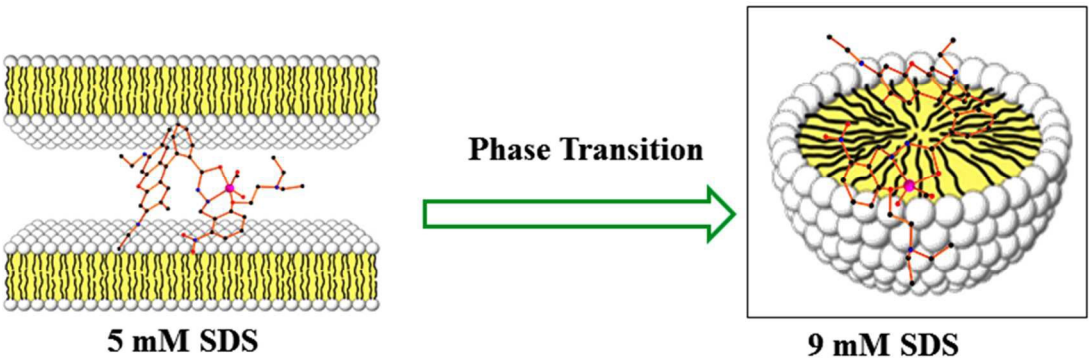

Scheme 2 Schematic presentation of interactions of **L**^{3}-Hg^{2+} with the laminar microstructure and miceller microstructure of SDS **(**adopted fromHttp://fig.cox.miami.edu/~cmallery/255/255chem/mcb2.20.micelle.jpg).

SEM and TEM Studies

Fig. 10

Fig. 11

At higher and lower magnifications of SEM studies at 9 mM SDS a core-shell structure is quite apparent, in which metallic part is embedded with ligand and SDS in a definite spherical Janus like structure (**Fig. 10**). This core-shell structure can also be explained by TEM studies; the inner core (dark black) of the particle comprises of metallic zone (**Fig. 11**) and outer shell by the ligand along with SDS which are in agglomerated condition by hydrophilic interactions. However, in presence of 5 mM SDS the probe undergoes extensive aggregation with no definite shape which is also prevailing from both SEM and TEM studies.

Analyst Accepted Manuscript

Cell Studies

Mitochondria are cytoplasmic organelles in eukaryotic cell and produce ATP (95%) required for the cell. In nerve cells mitochondrial function has very crucial role to supply high, long term and specific energy demand to regularizethe brain functions. Basic mechanism for mercury toxicity emerges from direct and indirect damage of mitochondria through reduction of glutathione due to extreme ROS (reactive organic species) generation and increased mitochondrial membrane permeability. Hence, there is a certain need to detect Hg^{2+} in its permissible limits to avoid its toxicity and also to apply for chelator based treatment to reduce Hg^{2+} poisoning in humans. In the present study we evaluate the chemo sensing capability of $\mathbf{L^3}$ to detect Hg^{2+}. The cytotoxic effects of $\mathbf{L^3}$ were determined by cell viability assay on HepG2 cells. Upto 50 μM it shows less than 30% cytotoxicity for $\mathbf{L^3}$ and more than 87% cells are viable upto dose of 20 μM (**Fig. S8**). Hence there no such significant cytotoxicity was observed upto 20 μM. Furthermore, we have performed the Hg^{2+} ion detection capability of $\mathbf{L^3}$ using *in vitro* fluorescence analysis in HepG2 cells (**Fig. 11**). The intracellular imaging of HepG2 cells treated with $\mathbf{L^3}$ ligand (10 μM) shows no intracellular fluorescence. Else, live cell imaging of HepG2 cells treated with equimolar amount of Hg^{2+} and $\mathbf{L^3}$ ligand shows the excellent intracellular cytoplasmic red fluorescence (**Fig. 12**).

Fig. 12

There a concentration dependent increase in the red fluorescence was noted indicating $\mathbf{L^3}$ as an excellent cytoplasmic Hg^{2+} tracker. We have observed that $\mathbf{L^3}$can sense low concentration of

Analyst Accepted Manuscript

Hg^{2+} ions present in the cytoplasm (2-8 μM). We didn't see any nuclear binding of Hg^{2+}-**L**^{3}; this may be due to the restricted permeability of **L**^{3} to cytoplasm (**Figure 12**). Hence presented ligand has low cytotoxicity and is biocompatible for cellular cytoplasmic Hg detection and can be used for Hg detection in the biological sample.

Conclusion

A new type of easily synthesizable rhodamine-based chemosensor with potential NO_2 donor atoms showed selective and rapid recognition of toxic Hg^{2+} ions. The binding stoichiometry of the sensor with Hg^{2+} was established by the combined Job's and HRMS (m/z) methods. All biologically relevant metal ions as well as toxic heavy metal ions and anions did not interfere with the detection of Hg^{2+} ion. The detection limit of Hg^{2+} calculated by 3σ method gives a value of 78 nM. Bio-compatibilityand good solubility in mostly aqueous medium (8:2, H_2O:MeCN) along with its cell permeability with no or negligible cytotoxicity provide a good opportunity towards *in-vitro*/ *in-vivo* cell imaging studies which showed cytoplasmic recognition of Hg^{2+} ions. Under optical microscope, heavily agglomerated microstructure for **L**^{3}-Hg^{2+} in 5 mM SDS changes to spherical shape in 9 mM SDS. Not only that we have also carried out the fluorescence titrations in the presence of SDS and also SDS concentration was varied at a fixed concentration of receptor and the guest. The presence of SDS causes enhanced quantum yield (φ) and more importantly the stability constant (K_f) by ~an order of magnitude compared to those in absence of SDS. Again, the FI of [**L**^{3}–Hg]$^{2+}$ complex is enhanced by 143 fold to that in absence of SDS. So an attempt was made to get some idea of the dependence of K_f on SDS concentration. It was interesting to see that a plot of K_f as function of [SDS] showed initial slow increase in K_f upto 6 mM of SDS and the then it picks rapidly indicating the

Analyst Accepted Manuscript

fact of aggregation induced emission enhancement (AIEE). All these observations clearly manifest enhanced rigidity of the $[\mathbf{L}^3–Hg]^{2+}$ in the heterogeneous micro-environment restricting to dynamic movement of the $[\mathbf{L}^3–Hg]^{2+}$ complex. The change in fluorescence anisotropy (r) with [SDS] is best described by change in morphology of the SDS microstructure from laminar to spherical shape; the former being more efficient to provide better rigidity to $[\mathbf{L}^3–Hg]^{2+}$ complex and hence higher r values at ~5 mM of SDS.

Acknowledgement

Financial support from the Department of Science and Technology (DST), Government of India, New Delhi (ref. number SR/S1/IC-20/2012) is gratefully acknowledged. Instrumental facilities FE-SEM from the Department of Physics (DST-FIST) Jadavpur University and TEM from the CRNN, University of Calcutta are gratefully acknowledged.

Notes and references

†Electronic Supplementary Information (ESI) on the synthesis and corresponding characterization data for compound $\mathbf{L}^3$ are available at DOI: 10.1039/b000000x/

References

1 S. Zhang, *Nat. Biotech,* 2003, **21**, 1171-1178.

2 L.Wang,L. L. Li,H. L.Ma, H.Wang, *Chin. Chem. Lett*., 2013, **24**, 351-358.

3 T. L.Greaves andC. J. Drummond, *Chem. Soc. Rev.,* 2013,**42**, 1096-1120.

Analyst Accepted Manuscript

4 T. Y. Ma, H.Li, Q. F. Deng, L.Liu, T. Z.Ren and Z. Y. Yuan, *Chem. Mater*., 2012,**24**, 2253-2255.

5 C. Lv, G.Xu andX.Chen,*Chem.Lett*., 2012, **41**, 1201-1203.

6 A. M.Percebom, J.Janiak, K.Schillén, L.Piculell and W.Loh, *Soft Matter*, 2013, **9**, 515-526.

7 Y. N.Guo, Y.Li, B.Zhi, D.Zhang, Y.Liu andQ.Huo,*RSC Adv.*, 2012, **2**, 5424-5429.

8 L. G.Chen andH.Bermudez, *Langmuir*, 2012, **28**, 1157-1162.

9 S. L.de-Rooy, S.Das, M.Li, B.El-Zahab, A.Jordan, R.Lodes, A.Weber, L.Chandler, G. A.Baker andI. M. Warner, *J. Phys. Chem. C*., 2012, **116**, 8251-8260.

10 Y.Liu, X.Feng, J.Shi, J.Zhi, B.Tong andY. Dong, *Chin. J.Polym. Sci.*, 2012, **30**, 443-450.

11 Y.Ren and T.Baumgartner, *Inorg. Chem*., 2012, **51**, 2669-2678.

12 X. Chen, Y.Xiang, P.Song, R.Wei, Z.Zhou, K.Li andA.Tong, *J. Lumin*., 2011, **131**, 1453-1459;

13 B.Xu, Z.Chi, X.Li, H.Li, W. Zhou, X.Zhang, C.Wang, Y.Zhang, S.Liu andJ. Xu, *J. Fluoresc.*, 2011, **21**, 433-441.

14 E.Lucenti, C.Botta, E.Cariati, S.Righetto, M.Scarpellini, E.Tordin andR.Ugo, *Dyes Pigment*., 2013, **96**, 748-755.

15 C.Shi, Z.Guo, Y.Yan, S.Zhu, Y.Xie, Y. S.Zhao, W.Zhu andH.Tian, *ACS Appl. Mater. Interfaces*, 2013, **5**, 192- 198;

16 P.Guo, S.Yan, Y.Zhou, C.Wang, X.Xu, X.Weng andX. Zhou, *Analyst*, 2013, **138,** 3365-3367.

17 W. Z.Yuan, Z. Q.Yu, P.Lu, C.Deng, J. W. Y.Lam, Z.Wang, E. Q.Chen, Y.Mad andB. Z. Tang, *J. Mater. Chem*., 2012, **22**, 3323-3326.

Analyst Accepted Manuscript

18 G.Yu, S.Yin, Y.Liu, J.Chen, X.Xu, X.Sun, D.Ma, X.Zhan, Q.Peng, Z.Shuai, B. Z.Tang, D.Zhu, W.Fang andY.Luo, *J. Am. Chem. Soc*., 2005, **127**, 6335-6346.

19 X.Gu, J.Yao, G.Zhang, C. Zhang, Y.Yan, Y.Zhao andD. Zhang,*Chem. Asian J.*, 2013,**8**, 2362-2369.

20 J.Luo, X.Wang, X.Wang andW. Su, *Chin. J.Chem.*, 2012, **30**, 2488-2494.

21 X.Zhou, H.Li, Z.Chi, B.Xu, X.Zhang, Y.Zhang, S.Liu andJ. Xu, *J. Fluorsc*., 2012, **22**, 565-572.

22 W.Wu, S.Ye, R.Tang, L.Huang, Q.Li, G.Yu, Y.Liu, J.Qin andZ. Li, *Polymer*, 2012, **53**, 3163- 3171.

23 B. K.An, S. K.Kwon, S. D.Jung andS. Y. Park,*J. Am. Chem. Soc.*, 2002, **124**, 14410-14415.

24 S. J.Li, B. K.An, S. D.Jung, M. A.Chung and S. Y. Park, *Angew. Chem., Int. Ed*., 2004, **43**, 6346-6350.

25 J. B. Birks, Wiley: London, 1970.

26 X. Cao, R. W.Tolbert, J. L.McHale andW. D. Edwards, Dye *J. Phys. Chem. A*1998, **102**, 2739–2748.

27 R.Badugu, J. R.Lakowicz andC. D. Geddes, *J. Am. Chem. Soc.* 2005, **127**, 3635–3641.

28 Y.Ren, J. W. Y.Lam, Y.Dong, B. Z.Tang andK. S. Wong, *J. Phys. Chem. B* 2005, **109**, 1135–1140.

29 H.Tong, Y.Dong, Y.Hong, M.Haussler, J. W. Y.Lam, H. H. Y.Sung, X.Yu, J.Sun, I. D.Williams, H. S.Kwok andB. Z. Tang, *J.Phys. Chem. C* 2007, **111**, 2287–2294.

30 Z.Li, Y.Dong, B.Mi, Y.Tang, M.Haussler, H.Tong, Y.Dong, J. W. Y.Lam, Y.Ren, H. H. Y.Sung, K. S.Wong, P.Gao, I. D.Williams, H. S.Kwok andB. Z. Tang, *J. Phys. Chem. B* 2005, **109**, 10061–10066.

Analyst Accepted Manuscript

31 L. S.Hung andC. H. Chen, *Mater. Sci. Eng.,* 2002, **39**, 143–222.

32 J. H.Burroughes, D. D. C.Bradley, A. R.Brown, R. N.Marks, K.Mackay, R. H.Friend, P. L.Burns andA. B. Holmes, *Nature* 1990, **347**, 539–541.

33 J.Chen, C. C. W.Law, J. W. Y.Lam, Y.Dong, S. M. F.Lo, I. D.Williams, D.Zhu andB. Z. Tang, *Chem. Mater.* 2003, **15**, 1535–1546.

34 M.Rosoff, Ed. *Vesicles*; Dekker: New York, 1996.

35 C. F. J.Faul, *Adv. Mater.* 2003, **15**, 673–683.

36 P.Bilski, R. N.Holt andC. F.Chignell, *J. Photochem. Photobiol., A* 1997, **110**, 67–74.

37 P.Bilksi andC. F. Chignell, *J. Photochem. Photobiol., A* 1994, **77**, 49–58.

38 H.Hachisako andR. Murakami, *Chem. Commun.* 2006, 1073–1075.

39 H.Hachisako, N.Ryu andR. Murakami, *Org. Biomol. Chem.* 2009, **7**, 2327–2337.

40 A. K.Chibisov, V. I.Prokhorenko andH.Go¨rner, *Chem. Phys.* 1999, **250**, 47–60.

41 A. K.Mandal andM. K. Pal, *Chem. Phys.* 2000, **253**, 115–124.

42 L.Tang, J.Jin, S.Zhang, Y.Mao, J.Sun, W.Yuan, H. Zhao, H.Xu, A.Qin andB. Tang, *Sci. China, Ser. B: Chem.* 2009, **52**, 755–759..

43 Y.F.Zhang, Q.Yuan, T.Chen, X. B.Zhang, Y.Chen andW. H. Tan, *Anal. Chem*. 2012, **84**,1956-1962.

44 E. S.Childress, C.A.Roberts, D. Y.Sherwood, C. L. M.LeGuyader andE. J. Harbron, *Anal.Chem*.2012, **84**, 1235-1239.

45 L.Deng, X. Y.Ouyang, J. Y.Jin, C.Ma, Y.Jiang, J.Zheng, J. S.Li, Y. H. W.Li, H.Tan andR. H. Yang,*Anal. Chem*. 2013, **85**, 8594-8600.

46 P. B.Tchounwou,W. K.Ayensu, N. Ninashvili andD.Sutton, *Environ.Toxicol.,* 2003, **18**, 149–175.

Analyst Accepted Manuscript

47 V. D. Bittner Jr., J. S.Echeverria, H. V.Woods, C.Aposhian, M. D.Naleway, R. K.Martin, N. J.; Mahurin and M. Cianciola, *Neurotoxicol.Teratol.*1998, **20,** 429–439.

48 F.Di Natale, A.Lancia, A.Molino, M.Di Natale, D. Karatzaand D.Musmarra, *J. Hazard. Mater*. 2006, **132**, 220;

49 Y.Gao, S.De Galan, A.DeBrauwere, W.Baeyens andM.Leermakers, *Talanta*2010, **82**, 1919-1923.

50 F.Moreno, T.Garcia-Barrera andJ. L. Gomez-Ariza, *Analyst* 2010,**135**, 2700-2705.

51 X.Chai, X.Chang, Z.Hu, Q.He, Z.Tu andZ. Li, *Talanta*2010, **82**, 1791-1796.

52 X.Fu, X.Chen, Z.Guo, C.Xie, L.Kong, J.Liu andX.Huang, *Anal.Chim. Acta*2011, **685**, 21-28.

53 J. R. Lakowicz, Principles of Fluorescence Spectroscopy, 3rd. ed., Springer, New York, 2006, 67.

54 Haugland, R. P. The Handbook: A Guide to Fuorescent Probes and Labeling Technologies, 10th ed., Invitrogen Corp., Karlsbad, CA, 2005.

55 H. Y.Lee,K. M. K.Swamy, J. Y.Jung, G. Kim andJ. Yoon ,*Sens. Actuators, B*2013, **182**, 530-537.

56 F.Wanga, S. W.Nama, Z.Guoa, S.Parka andJ. Yoona, *Sens. Actuators, B*2012, **161**, 948-953.

57 X.Chen, T.Pradhan, F. Wang, J. S.Kim andJ. Yoon, *Chem. Rev.*2012, **112**, 1910-1956.

58 K.Bera, A. K.Das, M.Nag andS. Basak,*Anal. Chem.*2014, **86**, 2740-2746.

59 V.Dujols, F.Ford and A. W. Czarnik, *J. Am. Chem. Soc.*1997, **119**, 7386–7387.

60 Haugland, R. P. The Handbook: A Guide to Fuorescent Probes and Labeling Technologies, 10th ed., Invitrogen Corp., Karlsbad, CA, 2005.

Analyst Accepted Manuscript

61 L.Huang, X.Wang, G.Xie, P.Xi, Z.Li, M.Xu, Y.Wu andD.Baib, *Dalton Trans.* 2010, **39**, 7894-7896.

62 R.Bhowmick, R.Alam, T.Mistri, D.Bhattacharya, P.Karmakar andM. Ali, *Appl. Mater. Interfaces*2015, **7**, 7476–7485.

63 C. R.Lohani, J. M.Kim, S. Y.Chung, J.Yoon andK. H. Lee, *Analyst* 2010, **135**, 2079-2084.

Analyst Accepted Manuscript

TOC

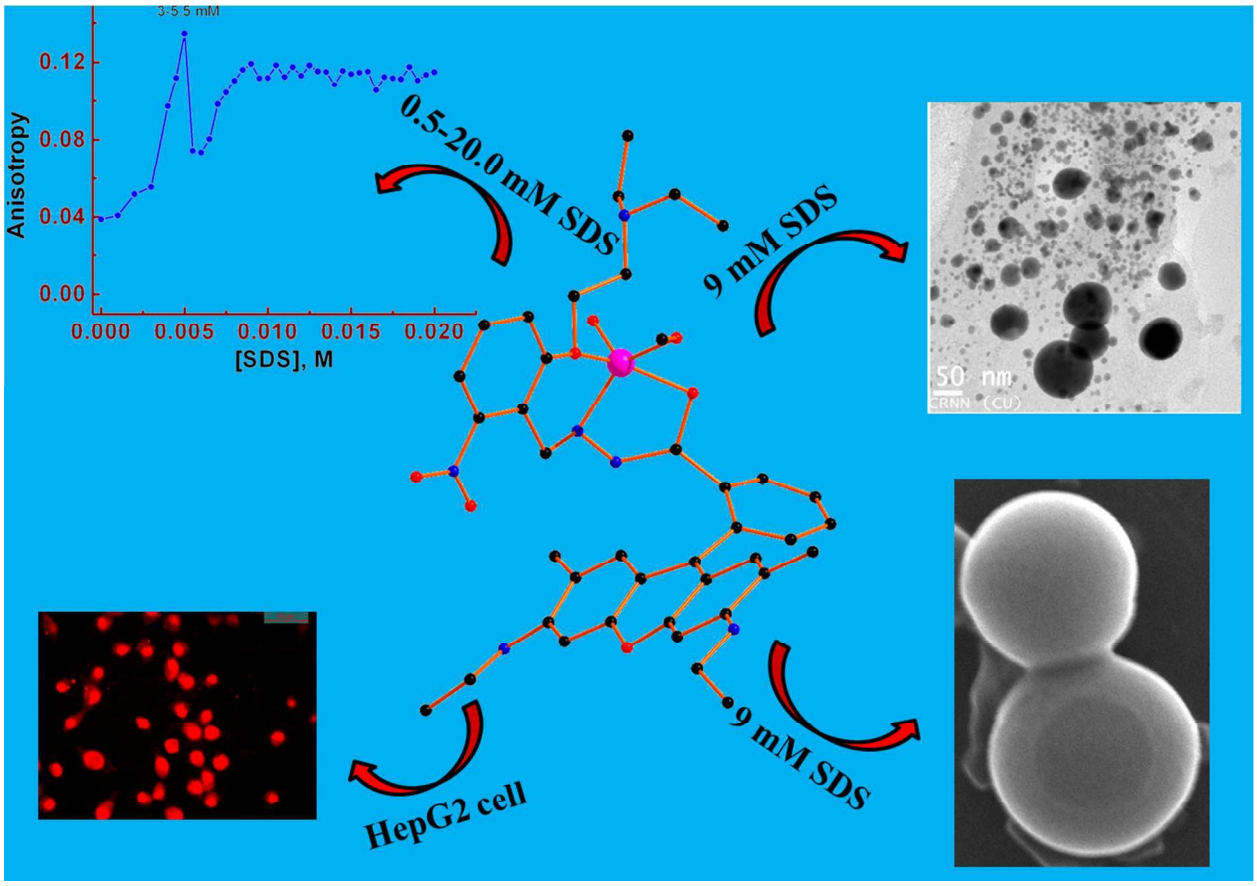

Analyst Accepted Manuscript

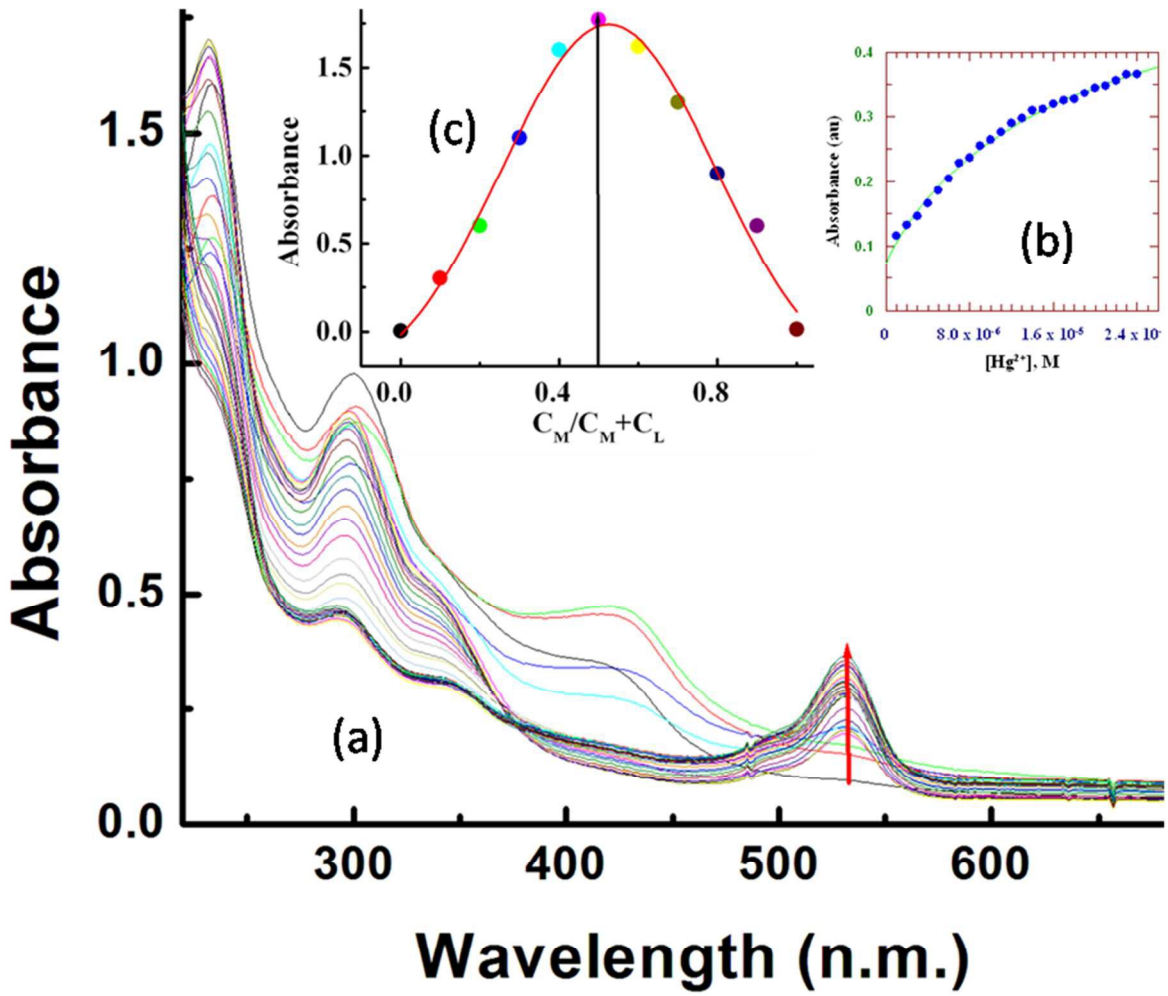

Fig. 1. (a)Absorption titration of L^3 (20.0 μM) with Hg^{2+} in MeCN-H_2O (2:8, v/v) in HEPES buffer (10 mM) at pH 7.2; (b) Non-linear fit of Absorbance vs. $[Hg^{2+}]$ plot at λ = 533 nm; (c)Job's plot for the determination of the composition of the L^3–Hg^{2+} complex

Analyst Accepted Manuscript

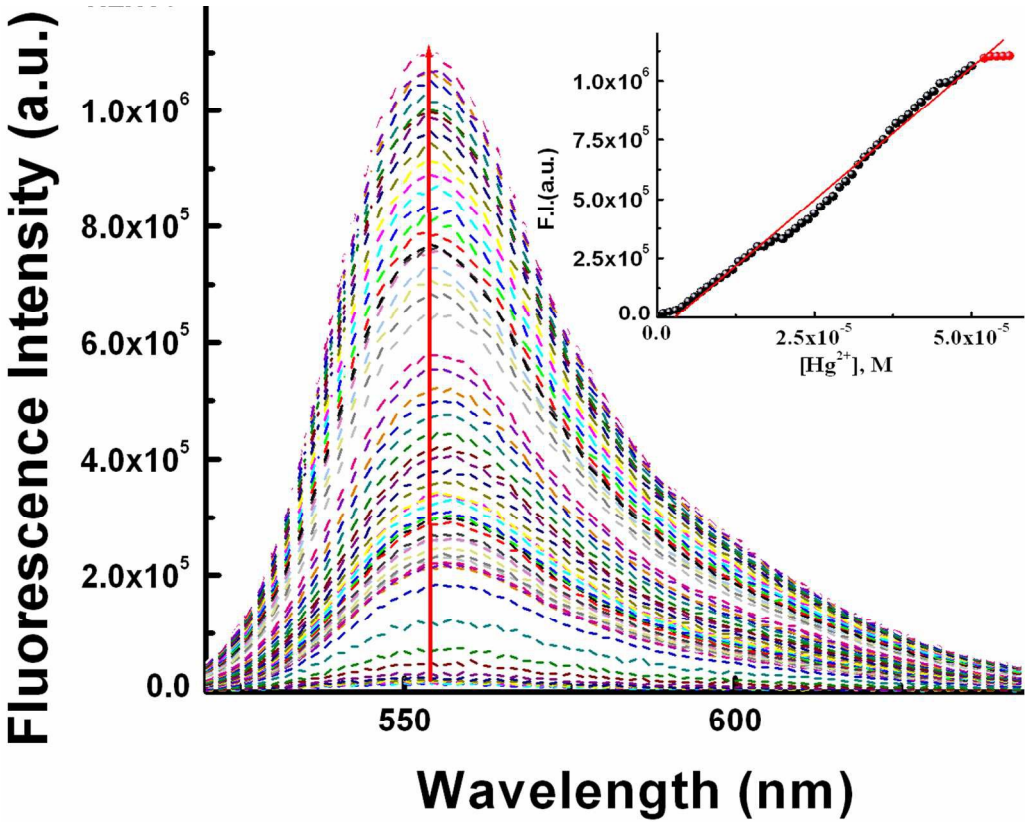

Fig. 2. Fluorescence titration of (10.0μM) in MeCN-H_2O (2:8, v/v) in HEPES buffer at pH 7.2 by the gradual addition Hg^{2+} with λ_{ex} = 510 nm, λ_{em} = 553 nm, Inset: linear fit of F.I vs. [Hg^{2+}] plot.

Analyst Accepted Manuscript

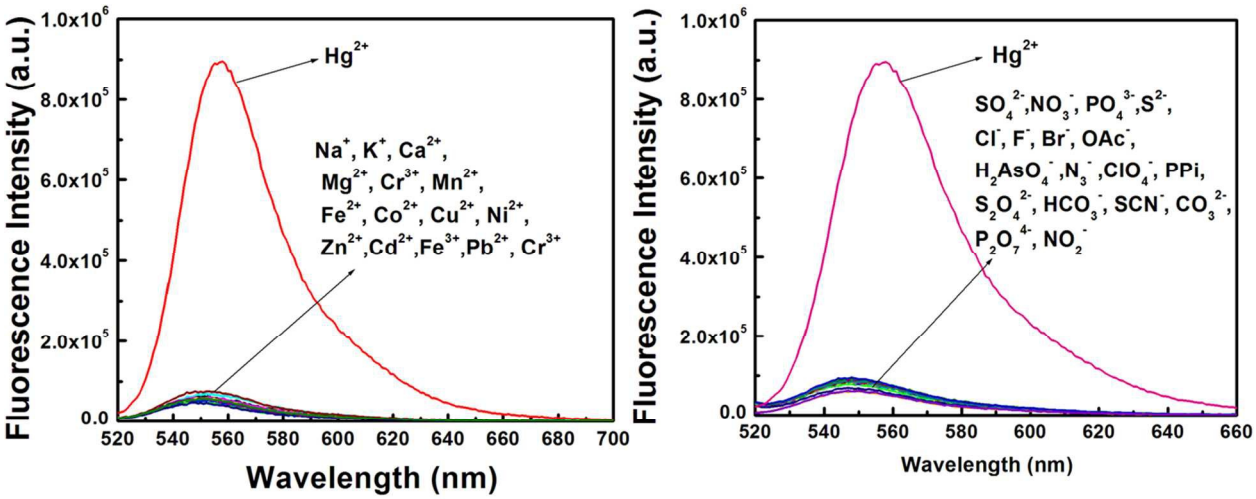

Fig. 3. Fluorescence emission induced by different cations and anions.

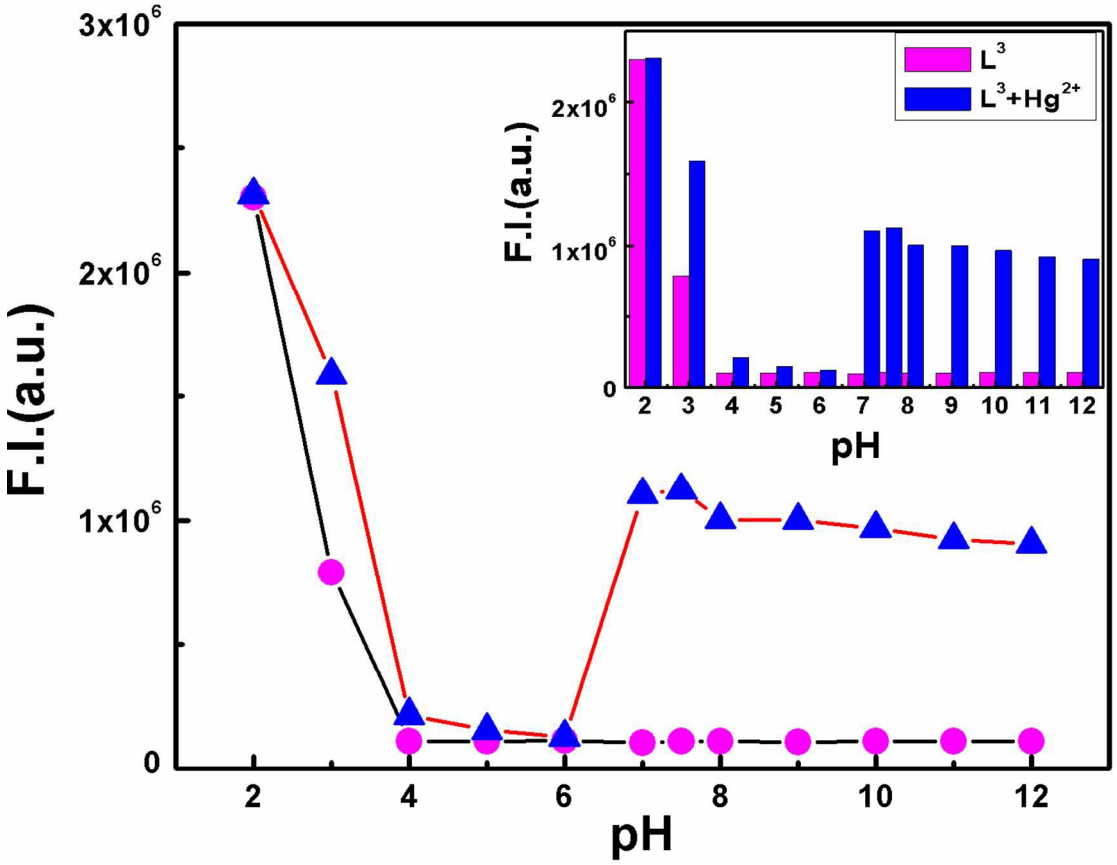

Fig. 4. pH dependent FIs of free ligand L^3 (magenta) and the L^3 –Hg^{2+} complex with L^3 :Hg^{2+}= 1:1.05 (blue) in the MeCN/H_2O (2:8 v/v) solvent system with λ_{ex} = 510 nm. The inset shows the histogram plot.

Analyst Accepted Manuscript

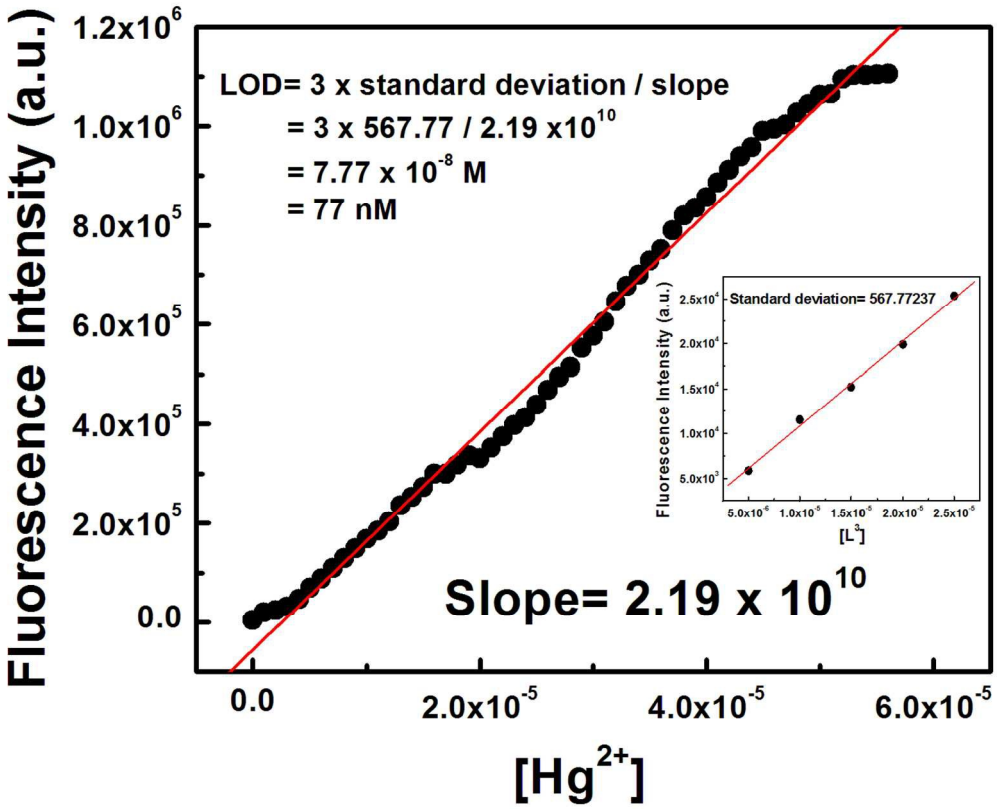

Fig. 5 Determination of Limit of detection (LOD) of Hg^{2+} by $\mathbf{L^3}$ from the slope of the plot of FI vs. $[Hg^{2+}]$ and the standard deviation of the blank (intercept) determined from the plot of FI vs. $[\mathbf{L^3}]$ utilizing 3σ method.

Analyst Accepted Manuscript

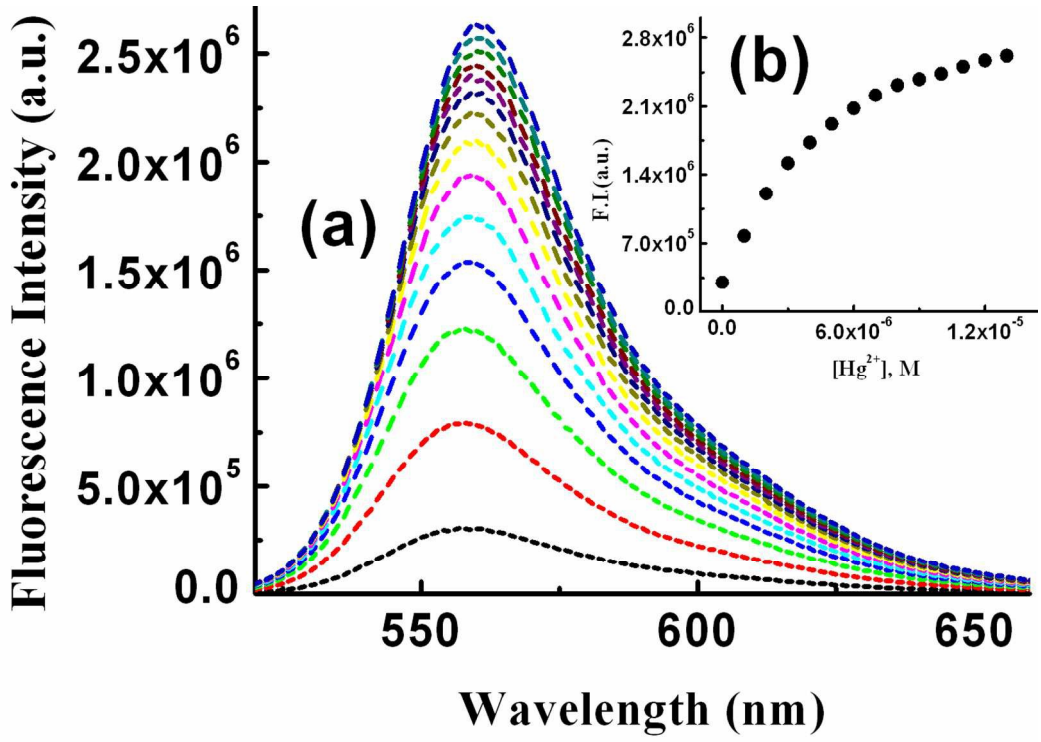

Fig. 6 (a) a) Fluorescence titration of $\mathbf{L^3}$ as a function of $[Hg^{2+}]$ at $[L^3]$ = 10 μM and [SDS] = 9.0 mM, in pure water; (b) Plot of FI vs. $[Hg^{2+}]$

Analyst Accepted Manuscript

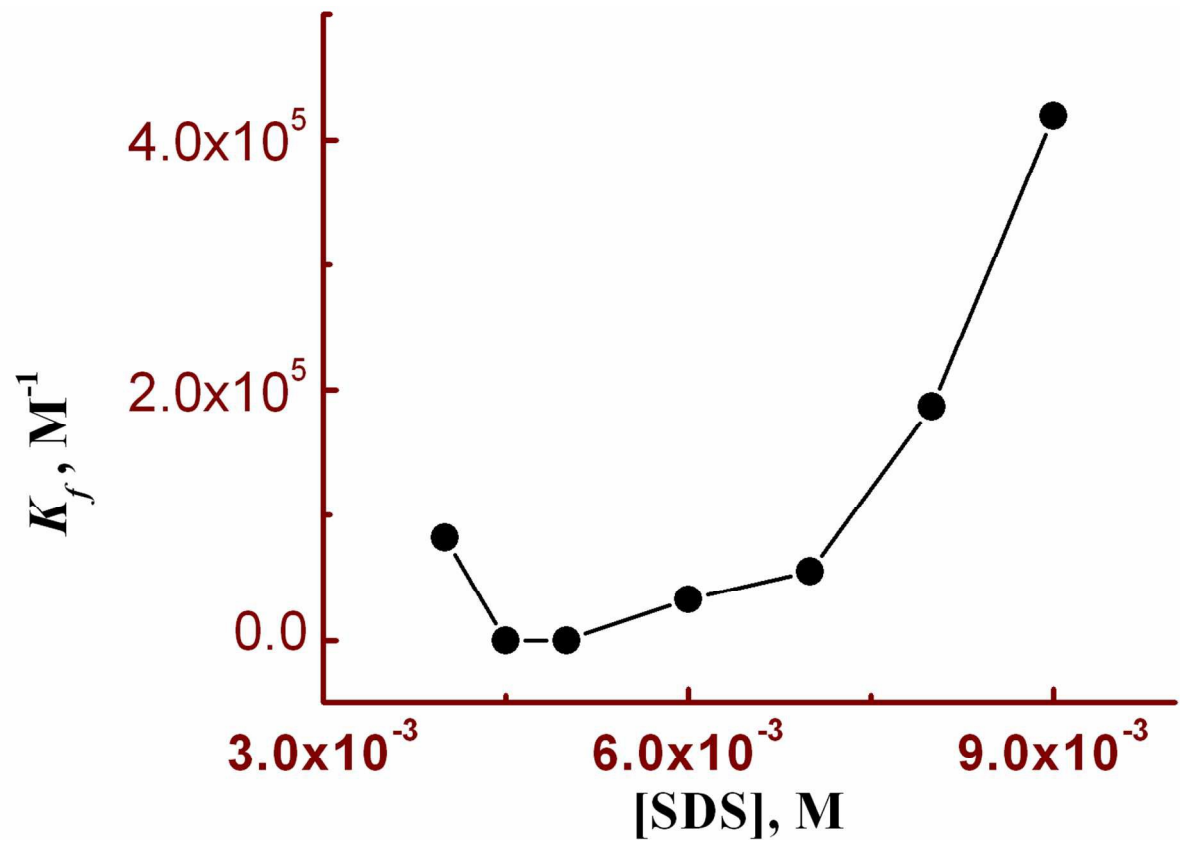

Fig. 7. A plot of K_f as a function of SDS concentration.

Analyst Accepted Manuscript

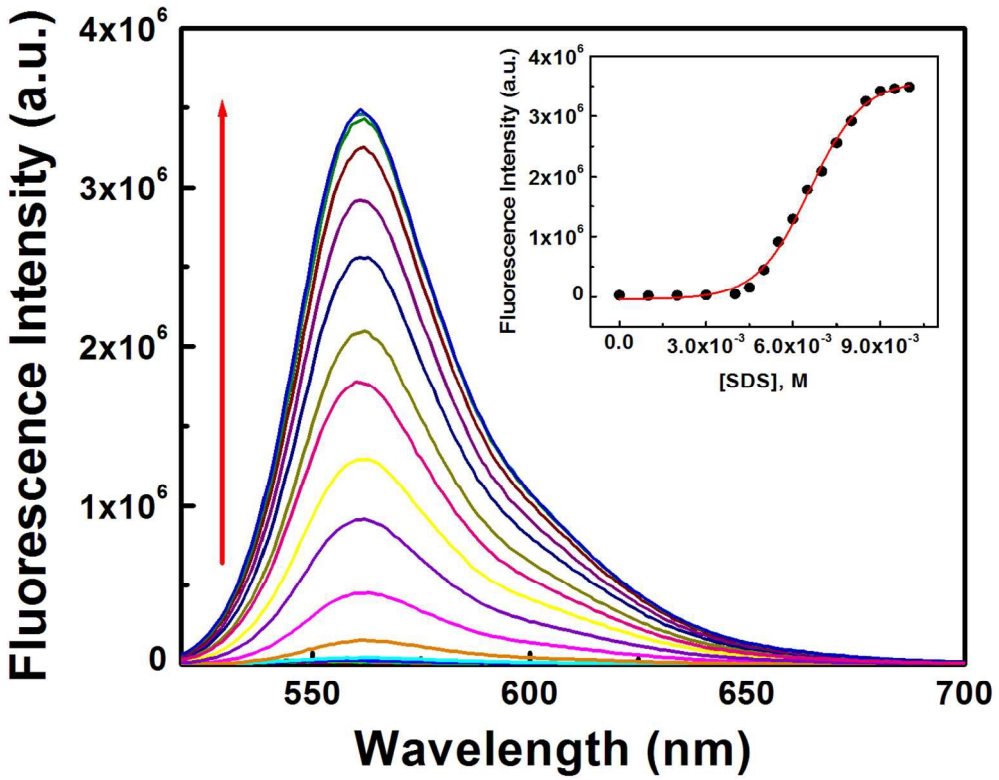

Fig. 8. Fluorescence titration as a function of [SDS] at [L^3] = 10 μM; [Hg^{2+}] = 10 μM, in pure water; Inset is the plot of FI vs. [SDS].

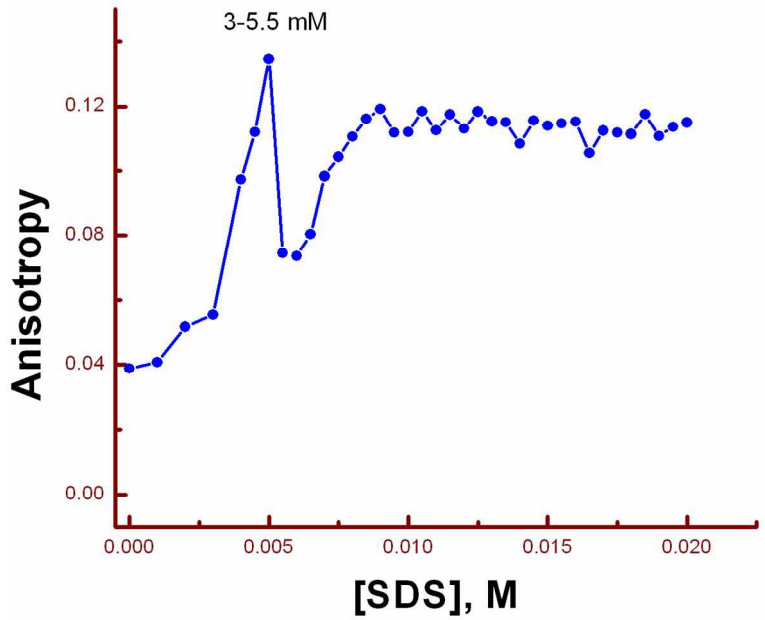

Fig. 9. A plot of anisotropy (r) as a function of SDS concentration.

Analyst Accepted Manuscript

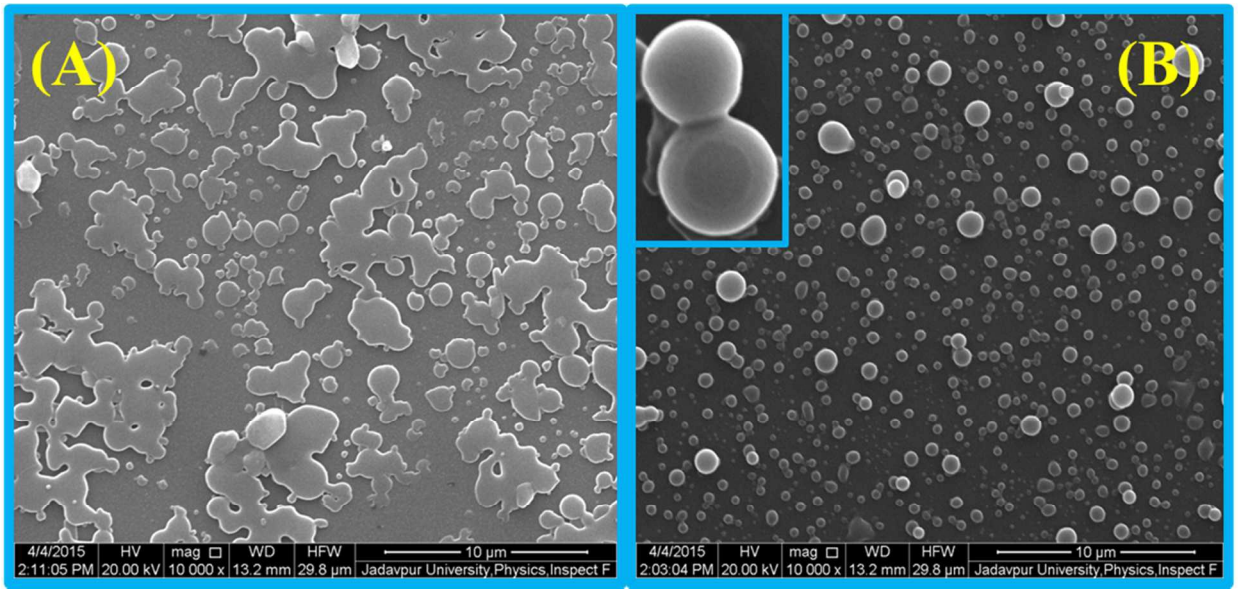

Fig. 10 SEM images of $\mathbf{L^3}$(10 µM)-Hg^{2+}(10 µM) in presence of (A) 5.0 mM SDS showing agglomerated microstructure with no particular shape and (B) 9.0 mM SDS with spherical microstructure.

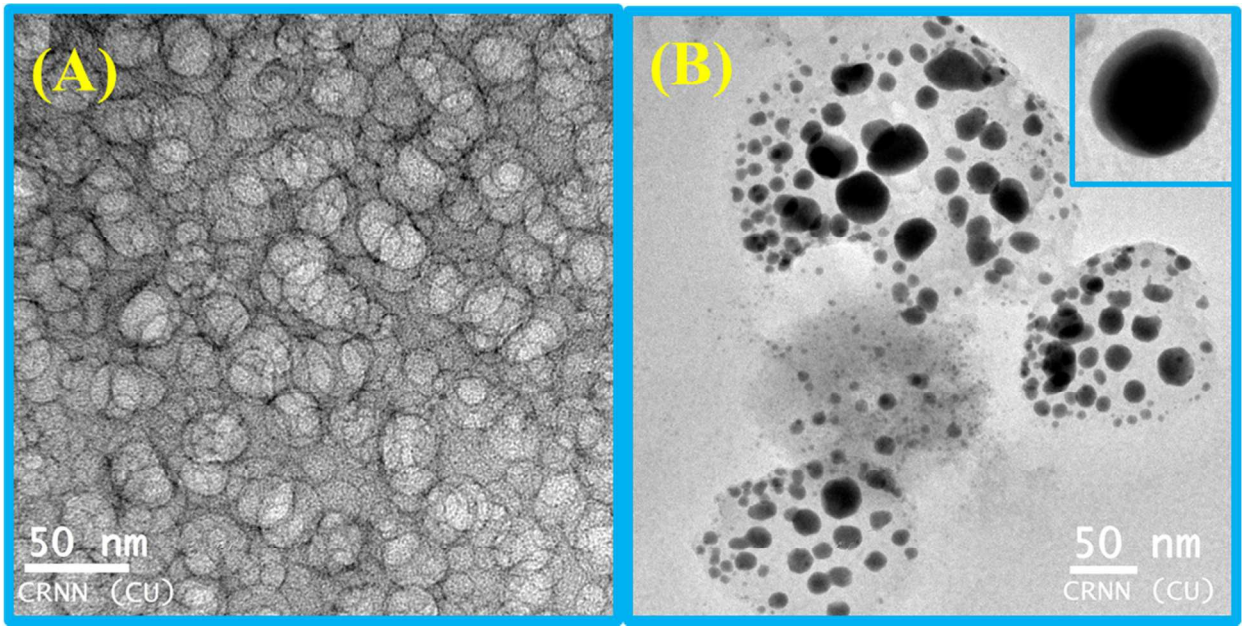

Fig. 11 TEM images of $\mathbf{L^3}$-Hg^{2+} in presence of (A) 5.0 mM SDS and (B) 9.0 mM SDS.

Analyst Accepted Manuscript

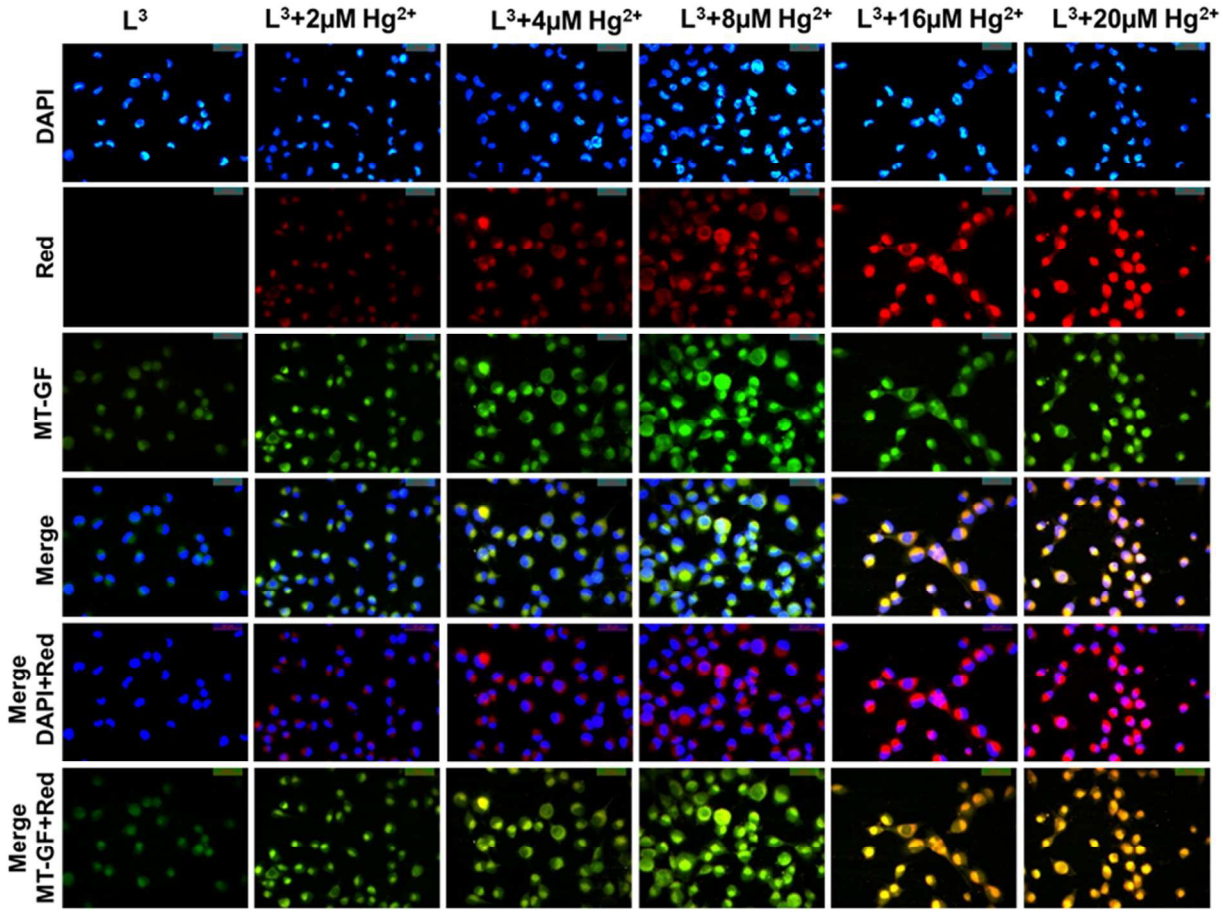

Fig. 12. Cell imaging studies of Hg^{2+} ions with $\mathbf{L^3}$**.** The fluorescence images of HepG2 cells were captured (40X) after incubated with 10 μM of $\mathbf{L^3}$ for 30 min at 37 °C, pre-incubated with (2, 4, 8, 16 and 20 μM) of Hg^{2+} for 3h at 37°C followed by washing thrice with 1X PBS. The image shows the strong cytoplasmic red florescence when $\mathbf{L^3}$ complexes with Hg^{2+} (Red). The merge images show the cytoplasmic $\mathbf{L^3}$-Hg^{2+} fluorescence and not in nucleus. Cytoplasmic complex formation was confirmed by DAPI (nuclear stain, blue) and MitoTrackerGreen FM (MT-GF, cytoplasm stain, Green).

Analyst Accepted Manuscript

Surfactant modulated aggregation induced enhancement of emission (AIEE)– a simple demonstration to maximize sensor activity

Rahul Bhowmick[a], Abu SalehMushaIslam[a], AtulKatarkar[b], Keya Chaudhuri[b] and Mahammad Ali[a],*

A rhodamine-based chemosensor, **L**^{3}, selectively and rapidly recognizes Hg^{2+} ion in presence of all biologically relevant metal ions and toxic heavy metals with detection limit of 78nM along with cytoplasmic cell imaging applications.The FI of [**L**^{3}–Hg]$^{2+}$ complex is unprecedentedly enhanced enormously (~143 fold) to that in absence of SDS and may be attributed to an aggregation induced emission enhancement (AIEE).

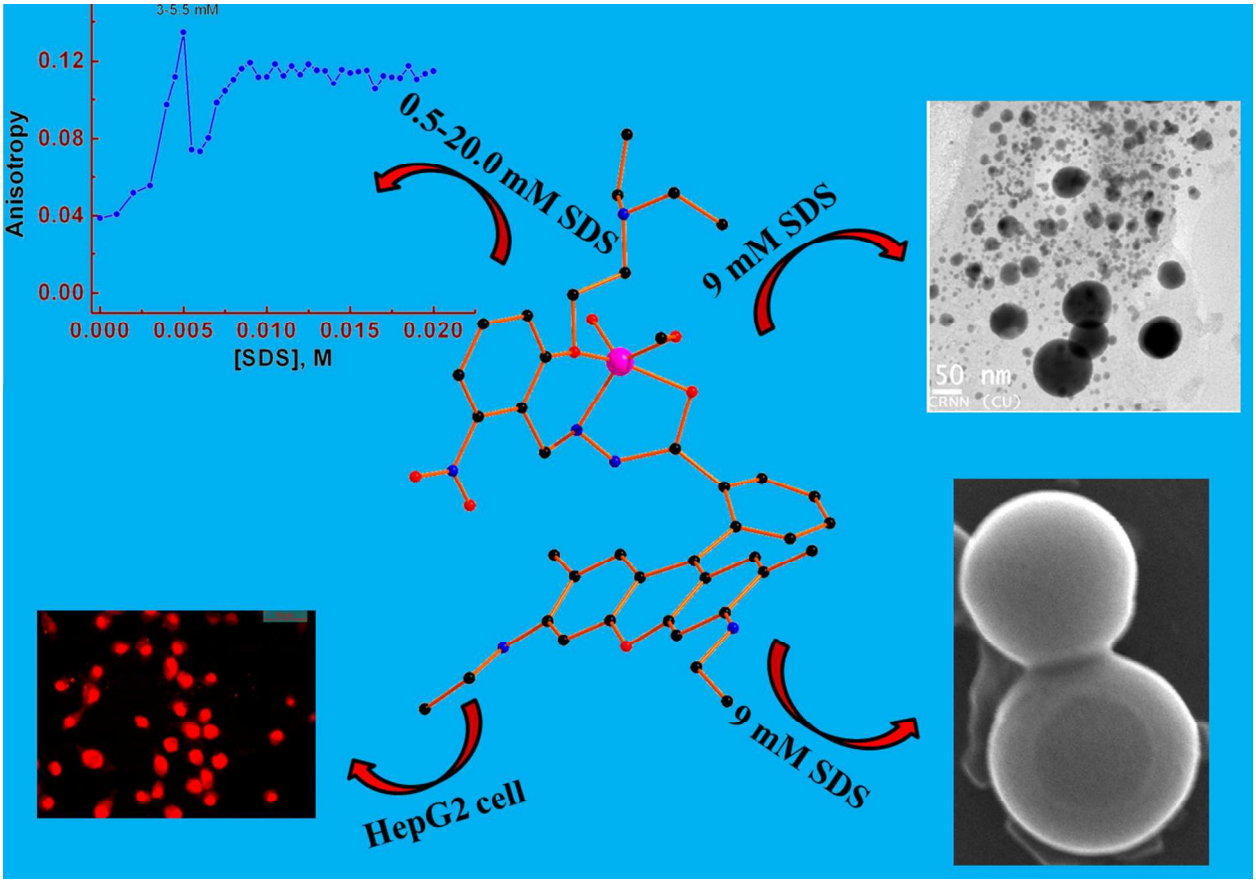

Analyst Accepted Manuscript

Analyst Accepted Manuscript